Attribution of Runoff Decline in the Amu Darya River in Central Asia during 1951–2007

XIAOLEI WANG,[+,#] YI LUO,[+,@] LIN SUN,[+] CHANSHENG HE,[&] YIQING ZHANG,[+,#] AND SHIYIN LIU[**]

[+] *Key Lab of Ecosystem Network Observation and Modeling, Institute of Geographical Sciences and Natural Resources Research, Chinese Academy of Sciences, Beijing, China*
[#] *University of Chinese Academy of Sciences, Beijing, China*
[@] *Xinjiang Institute of Ecology and Geography, Chinese Academy of Sciences, Urumqi, China*
[&] *Department of Geography, Western Michigan University, Kalamazoo, Michigan*
[**] *Cold and Arid Regions Environmental and Engineering Research Institute, Chinese Academy of Sciences, Lanzhou, China*

(Manuscript received 30 June 2015, in final form 19 January 2016)

ABSTRACT

Runoff in the Amu Darya River (ADR) in central Asia has been declining steadily since the 1950s. The reasons for this decline are ambiguous, requiring a complete analysis of glaciohydrological processes across the entire data-scarce source region. In this study, grid databases of precipitation from the Asian Precipitation–Highly Resolved Observational Data Integration Toward Evaluation of Water Resources (APHRODITE) and temperature from Princeton's Global Meteorological Forcing Dataset (PGMFD) are used to force the distributed, glacier-enhanced Soil and Water Assessment Tool (SWAT) model to simulate glaciohydrological processes for 1951–2007 so as to determine long-term streamflow changes and the primary driving factors in the source region of the ADR. The study suggests that the database was a suitable proxy for temperature and precipitation forcing in simulating glaciohydrological processes in the data-scarce alpine catchment region. The estimated annual streamflow of 72.6 km^3 in the upper ADR had a decreasing trend for the period from 1951 to 2007. Change in precipitation, rather than in temperature, dominated the decline in streamflow in either the tributaries or mainstream of the ADR. The streamflow decreased by 15.5% because of the decline in precipitation but only increased by 0.2% as a result of the increase in temperature. Thus, warming temperature had much less effect than declining precipitation on streamflow decline in the ADR in central Asia in 1951–2007.

1. Introduction

The Amu Darya River (ADR) is the largest river in the Aral Sea basin, with a share of mountain discharge greater than 90%. The ADR supplies water to a large population and to the Aral Sea in the downstream region, accounting for two-thirds of total runoff in the Aral Sea basin (Agal'tseva et al. 2011). Water availability in the ADR is of international importance because of water conflicts among countries in this region and the deteriorating Aral Sea environment. Streamflow in the ADR has been declining since the middle of the last century (Stulina and Eshchanov 2013), with a pessimistic future for the water supply in the glacierized catchments of central Asia (Sorg et al. 2014).

Most studies on the ADR have concentrated on its glacierized tributaries (e.g., the source regions of the Pyanj and Vakhsh Rivers), especially in terms of the impact of climate change on future glaciohydrological processes. Hagg et al. (2013) observed a slight reduction in annual runoff in Rukhk catchment—a small river in the upper Pyanj catchment. Kure et al. (2013) projected an increase in annual mean river discharge in the snow-/glacier-dominated areas of Pyanj and Vakhsh Rivers

Supplemental information related to this paper is available at the Journals Online website: http://dx.doi.org/10.1175/JHM-D-15-0114.s1.

Corresponding author address: Yi Luo, Key Lab of Ecosystem Network Observation and Modeling, Institute of Geographical Sciences and Natural Resources Research, Chinese Academy of Sciences, 11A, Datun Road, Chaoyang District, 100101 Beijing, China.
E-mail: luoyi@igsnrr.ac.cn

DOI: 10.1175/JHM-D-15-0114.1

until 2060 due to increasing air temperature, followed by a decrease due to the subsequent disappearance of small glaciers. However, there are rarely any reports on either past or future variations in streamflow of the entire ADR. In the past two decades, there have been contrasting reports on trends in precipitation in central Asia. This is attributed partly to the limited meteorological stations in the high mountain area and to the dysfunction of a number of the stations since 1990 (Sorg et al. 2012). Thus, estimation of changes in precipitation in its alpine watersheds remains highly uncertain.

Changes in river runoff can be determined using statistical techniques based on observed hydrological and meteorological data (Unger-Shayesteh et al. 2013). Statistical techniques are adopted to test the trend of change or to establish regression relations between runoff and temperature or precipitation observed at lower points in the data-scarce high alpine watersheds (Aizen et al. 1997; Nezlin et al. 2004; Savitskiy et al. 2008). These statistically based relations may not discern the complex mechanisms of precipitation–streamflow transformations in glacierized watersheds and thereby fail to capture the reasons for changes in runoff due to changes in precipitation and/or temperature. In the glacierized watersheds, part of the seasonal precipitation could be stored in the glacier and then released as meltwater with years of delay (Unger-Shayesteh et al. 2013). This may induce further difficulties in determining the reasons for changes in streamflow through statistically based relations.

Change in snow/glacier melt due to rising temperatures was usually regarded as the primary reason for change in river runoff (Savitskiy et al. 2008; Olsson et al. 2010). Change in meltwater could explain change in streamflow only in the glacierized subbasins (e.g., Pyanj and Vakhsh Rivers), rather than in the entire watersheds (e.g., the ADR basin). While snow/glacier melt dominates river inflow in mountainous river basins (Froebrich and Kayumov 2004), climate change (including changes in temperature and precipitation) severely affects such melt characteristics (Barnett et al. 2005; Immerzeel et al. 2010). The physically based glaciohydrological models can investigate the pattern changes in streamflow and reveal the combined impact of temperature and precipitation on the individual tributaries of the ADR basin. Furthermore, integrative analysis of individual subbasins with different water balance components could reveal the stream change patterns and attribute the changes for the entire ADR. Distributed hydrological models upgraded with glacial processes modules could become an effective tool for investigating long-term variations in different runoff components with high temporal resolutions (Unger-Shayesteh et al. 2013). Comprehensive attribution studies could be performed after obtaining all of the runoff components, including ice melt. The models such as Spatial Processes in Hydrology (SPHY; Lutz et al. 2014), Hydrologic Engineering Center Hydrologic Modeling System (HEC-HMS; Kure et al. 2013), Hydrologiska Byråns Vattenbalansavdelning (HBV)–ETH (Hagg et al. 2007, 2013) and the glacier-enhanced Soil and Water Assessment Tool (SWAT; Luo et al. 2013) have been used to simulate runoff in the headwater regions of glacier and snowmelt-fed rivers, such as the Pyanj and Vakhsh Rivers, the Sary-Djaz–Kumaric River (Wang et al. 2015), the Syr Darya River (Gan et al. 2015), and the Chu River (Ma et al. 2015) in central Asia. These models have also been applied in other glacier-/snowmelt-dominated rivers in the world, laying a solid foundation for the contribution of climatic change to runoff change in the ADR basin.

In data-scarce situations, the reanalysis or interpolation data based on observations at meteorological stations are widely used as a proxy for precipitation to force the simulation of the hydrological processes in alpine watersheds. For example, Asian Precipitation–Highly Resolved Observational Data Integration Toward Evaluation of Water Resources (APHRODITE) precipitation data were used in watersheds in central Asia (Lutz et al. 2013) and the Hindu Kush–Karakoram–Himalaya (Immerzeel et al. 2012; Lutz et al. 2014) and in the Kaidu River of the Tian Shan by Li et al. (2014). The reliability of station-dependent grid databases varies with the number of meteorological stations and data quality. The gridded products often incorporate observations from only a few stations in central Asia, primarily located in the lowlands and therefore rendering regionalized results quite uncertain, especially for headwater catchment regions (Unger-Shayesteh et al. 2013). In particular, several Soviet-era stations have become dysfunctional since the 1990s, potentially increasing uncertainty in the grid database. It is therefore crucial to explore the usability of the grid database in data-scarce alpine watersheds in central Asia.

For the glacierized headwater region of the ADR basin, the reasons for the decline in streamflow since the 1950s are still unclear. Is it that the decline is dominated by changes in glacier melt? Which of the climatic factors (precipitation or temperature) dominantly drives the changes in meltwater and streamflow in the region? This study attempts to address these critical issues by using a glaciohydrological model and gridded climatic data in the headwater region of the ADR and its tributaries, where spatial distributions of both climate and glacier coverage are highly heterogeneous.

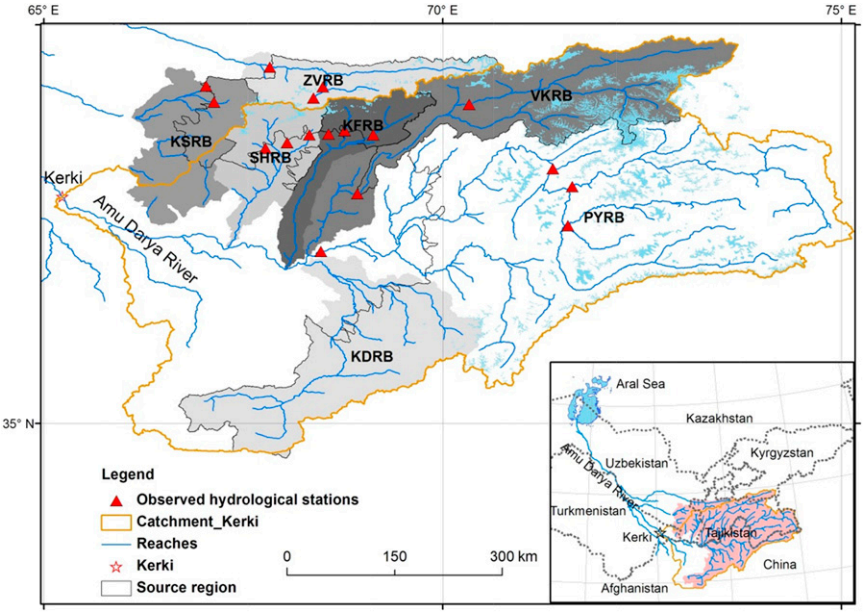

FIG. 1. Map of the UADRB in central Asia.

2. Materials and methods

a. The watershed

The ADR, which originates from the glaciers/snow fields of western Tian Shan and Pamir–Alai Mountains, flows nearly 2400 km from the mountains across the Karakum Desert and into the Aral Sea (Fig. 1). It consists of seven primary tributary basins: Pyanj (PYRB), Vakhsh (VKRB), Kafirnigan (KFRB), Surkhandarya (SHRB), Zeravshan (ZVRB), Kashka Darya (KSRB), and Kunduz (KDRB). After the confluence of PYRB and VKRB, the river runs along the border between Afghanistan and Uzbekistan, passing across Turkmenistan before again returning to Uzbekistan and the finally emptying into the Aral Sea. Two large tributaries on the right-hand side (KFRB and SHRB) and one on the left-hand side (KDRB) empty into the middle reaches of the ADR. Based on the hydrogeographical conditions of the area, two other rivers in the right-hand side (ZVRB and KSRB) are also tributaries of the ADR. Although some of the tributaries do not currently contribute to flow in the mainstream because of overwithdrawal (Olsson et al. 2010), they are still considered part of the ADR in this study.

Approximately 200 000 km^2 of the upper ADR basin (UADRB; also described as the source region of ADR in this text) is in the Pamir–Alai range. The elevation of the source region ranges is 1200–7400 m MSL, with some individual peaks exceeding 6000 m MSL.

The source region is rich in glaciers, which are unevenly distributed in the headwater catchments of the tributaries. There is a total area of 11 122 km^2 of glaciers in the ADR basin, of which ~91% are concentrated in the PYRB and VKRB. The glacier coverage ratio (GAR; which is expressed as glacier area to the catchment area) varies significantly among the headwaters. The GAR values of PYRB, VKRB, and ZVRB are 5.8%, 12.1%, and 6.3%, while those for KFRB, SHRB, KSRB, and KDRB are only 1.8%, 1.5%, 0.3%, and 0.4%, respectively.

The ADR basin has a continental climate that is primarily controlled by the westerlies—prevailing winds from the west toward the east in the midlatitudes of 30°–60°. Average annual precipitation exceeds 1000 mm in the alpine area, but only 100 mm in the foothills and adjacent plains. About 80% of the precipitation falls primarily in winter and early spring, when it is cold, with a mean temperature as low as −30°C. It is dry and hot in summer and early autumn, with a mean temperature as high as 30°C in July. Snow falls in winter and spring and thereafter melts as an important source of streamflow.

While ~80% of the runoff is concentrated in April–September, only 13% occurs in December–February (Agal'tseva et al. 2011). The PYRB and VKRB contribute some 70% of the flow volume of the mainstream, and the other tributaries combined contribute the remaining 30%. Table 1 lists the basic physical features of the headwater catchments of tributaries of the ADR.

b. The glacier-enhanced SWAT model

SWAT is a comprehensive, semidistributed, process-based river basin model that is widely used under a

TABLE 1. Physical features of source regions in the ADR and its primary tributaries in central Asia.

	Source area (km^2)	Glacier		Mean elev		Mean annual value	
		Area (km^2)	Ratio (%)	Source area (m MSL)	Glacier (m MSL)	T (°C)	P (mm)
PYRB	106 225	6199	5.8	3716	4908	−1.50	364
VKRB	32 380	3909	12.1	3805	4685	−3.36	594
KFRB	6035	107	1.8	2673	3788	2.79	1019
SHRB	6170	94	1.5	2572	3870	1.65	663
ZVRB	10 561	664	6.3	3192	4102	−0.03	579
KSRB	5846	18	0.3	2500	3810	4.68	458
KDRB	31 853	131	0.4	3037	4785	4.30	370
UADRB	199 070	11 122	5.6	3050	4250	−0.45	502

variety of climatic, soil, topographic, and management conditions (Arnold et al. 2012; Gassman et al. 2007). The SWAT model delineates a basin into subbasins and uses hydrological response units (HRUs) to account for the spatial heterogeneities of climate, land use and cover, soil, and topography within subbasins. An HRU is a combination of unique land-use type, soil type, and topographic slope. Land surface hydrological processes are simulated for each HRU, and the flow with sediments, nutrients, and pollutants is routed to subbasin outlets via tributaries and then to the basin outlet via the main channel. However, the flow has no dynamic hydrologic routing across the land surface but is discharged directly to the stream using a lagging equation. The detailed modeling and theoretical concepts of SWAT are documented by Neitsch et al. (2011).

The officially released versions of SWAT do not simulate glacier hydrology. Luo et al. (2013) proposed a glacier hydrological response unit (GHRU) approach and developed a glacier hydrology module for SWAT to simulate glaciohydrological processes at watershed scale. Each GHRU consists of an individual glacier. The module simulates the mass balance and dynamics for each GHRU. A GHRU is divided into elevation bands of equal intervals, and then the mass balance is simulated with respect to each band. The mass balance of a glacier is the sum of the balance of the bands. The glacier area change is derived from a volume–area scaling relation (Chen and Ohmura 1990) expressed as

$$A_{\mathrm{gla}} = (V_{\mathrm{gla}}/m)^{1/n}, \tag{1}$$

where A_{gla} (km^2) and V_{gla} (km^3) are glacier surface area and volume, respectively, and m and n are constants derived from glacier measurements. Following Bahr et al. (2015) and Liu et al. (2003), m is set at 0.04 and n is set at 1.35 in this study. It is assumed that the glacier retreats or advances from the lowest band upward or downward. The glacier mass balance components consist of mass accumulation and ablation. Ablation consists of sublimation and supraglacial snowmelt and ice melt. The ice melt and snowmelt are simulated using the degree-day factor method.

In this model, runoff in each HRU or GHRU is from rainfall, snowmelt, and glacier melt. Glacier melt includes supraglacial snowmelt, ice melt, and direct runoff generated from rainfall on ice. Also, a portion of the snowmelt and rainfall infiltrates the soil profile; some of the infiltration leaves the soil profile as lateral flow, and some recharges the aquifer and aquifer storage is released as base flow. In the officially released SWAT code, base flow is simulated in a linear outflow equation for only the shallow aquifer. The deficiency of this approach is that streamflow recedes to almost zero through winter season for rivers in the study area. Thus, Luo et al. (2012) adapted the model to allow both shallow and deep aquifers to release base flow. The shallow aquifer is treated as a quick pool and the deep aquifer as a slow pool, but the shallow aquifer could also recharge the deep aquifer. Base flow is simulated by a set of linear outflow equations of both the quick and slow pools. Using this approach, the simulation of streamflow during low-flow period is improved significantly. Surface runoff, lateral flow, and base flow are routed via tributary channels to the outlet of each subbasin and to the outlet of the basin via the primary channel, and channel water loss is removed from routed river discharge. Further details on the glacier-enhanced SWAT model are documented by Luo et al. (2013). This version of the SWAT model has been used in the headwater hydrological processes of the Manas River (Luo et al. 2013) and Kumaric River (Wang et al. 2015) in the Tian Shan range in China and in Chu River (Ma et al. 2015) and Naryn River (Gan et al. 2015) in the Tian Shan range in central Asia.

c. *Data and model setup*

1) INPUT SPATIAL DATA

The spatial data required to set up the model include digital elevation models [DEMs; Shuttle Radar

Topography Mission DEM with a spatial resolution of 90 m and 3 arc s (SRTM3)], land-use map, soil map, and glacier inventory. While daily meteorological data are required to force the simulation, discharge data at the outlet gauges are used to calibrate and validate the model. In addition, glacier area change data are used to restrict the parameterization of glacierized catchments. The sources and detailed processing of the spatial data (including glacier database compilation) are given in Text S1 of the supplemental material.

2) SWAT MODEL SETUP

The upstream boundaries of the ADR basin were delineated from the DEM map using ArcSWAT, which is an integrated platform of the SWAT model and ArcGIS software. In all, the UADRB was divided into 2747 subbasins and 19 253 HRUs. GHRUs were created for each glacier, including 6240, 2207, 751, 268, 250, 44, and 266 GHRUs in PYRB, VKRB, ZVRB, KFRB, SHRB, KSRB, and KDRB, respectively.

3) MODEL PARAMETERIZATION

Monthly streamflow data from 17 hydrological stations (Fig. 1) are used for independent calibration and validation purposes, as shown in Table S3 in the supplemental material. The Nash–Sutcliffe efficiency (NSE), percent bias (PBIAS), and squared correlation coefficient R^2 are used to evaluate model performance during calibration and validation (Moriasi et al. 2007).

For parameterization of glacierized basins, calibration can be wrong if the model is tuned with runoff data as the only target function. Including glacier mass balance and snow data as additional criteria significantly reduces parameter uncertainty (Hagg et al. 2013). Given that the availability of glacier mass balance data are present for only limited benchmark glaciers, using glacier area change (based on different phases of glacier data) as auxiliary data may constrain parameter uncertainty during calibration.

The parameter calibration is as follows: 1) adjust glacier melt parameters and check NSE and PBIAS during calibration and 2) run the model for the period 1960–2000 and check simulated glacier area change against the observed value. If the simulated value matches well with the observed one, then 3) adjust other parameters to improve PBIAS; if not, go back to the first step and readjust glacier parameters. This loop could be repeated quite a few times to get acceptable values of NSE, PBIAS, and glacier area change. Calibration is manually done by the trial and error method. During the calibration and validation, glacier melt and snowmelt, glacier area change, streamflow, water balance, etc. are monitored to ensure a rational simulation and water balance. Wherein PBIAS is still unacceptable, 4) the precipitation lapse rate (PLAPS) profile is next adjusted. Then, the loop from the first to the fourth step is repeated until reasonable results are obtained.

d. Climate input scheme

1) DATA SOURCE

Monthly observation data from 59 meteorological stations are obtained from the National Snow and Ice Data Center (NSIDC). The data series, which spans 1930–2000 (with gaps), is used to assess the quality of the gridded data. A large number of observations are discontinued because of the disintegration of the Soviet Union in the 1990s (Unger-Shayesteh et al. 2013). Meteorological observations for high-altitude mountains are scarce not only in central Asia, but also around the world. Thus, gridded databases with continuous spatial coverage and long time spans are increasingly used in simulating hydrological processes in the alpine watershed (Hagg et al. 2013; Immerzeel et al. 2012; Lutz et al. 2013, 2014). In this study, daily precipitation from APHRODITE and daily temperatures from Princeton's Global Meteorological Forcing Dataset (PGMFD; Sheffield et al. 2006) are used to force the glacier-enhanced SWAT model simulation.

The APHRODITE Monsoon Asia, version 1101, database (Yatagai et al. 2012) consists of long-term continental-scale daily gridded data for 1951–2007 that are based on a dense network of rain gauges with a spatial resolution of 0.25°. PGMFD is constructed by the combination of a suite of global observation-based datasets reanalyzed by the National Centers for Environmental Prediction–National Center for Atmospheric Research (NCEP–NCAR). The dataset has a daily resolution and a spatial scale of 0.5°, and it includes mean air temperature and minimum and maximum temperatures for 1948–2010. The temperature data are downscaled to 0.25° via bilinear interpolation, which is compatible with APHRODITE precipitation data in terms of spatial resolution.

Thus, 406 grid cells of temperature and precipitation data mask the UADRB, with 248, 66, 17, 23, 18, 34, and 57 grid cells in PYRB, VKRB, ZVRB, KFRB, SHRB, KSRB, and KDRB, respectively (Fig. 2).

Regression analysis is used to evaluate the gridded data against observations at the meteorological stations. In the grid cell to station comparison of monthly precipitation, R^2 is greater than 0.5, except for two stations (see Fig. S2a in the supplemental material). Then R^2 for monthly average temperature is above 0.97 (Fig. S2b). Overall, the R^2 values are 0.76 and 0.74 for monthly and annual precipitation, respectively (Figs. S2c,d). Then the R^2 values are 0.93 and 0.89 for mean monthly and annual temperature, respectively (Figs. S2e,f). Based on Moriasi et al.

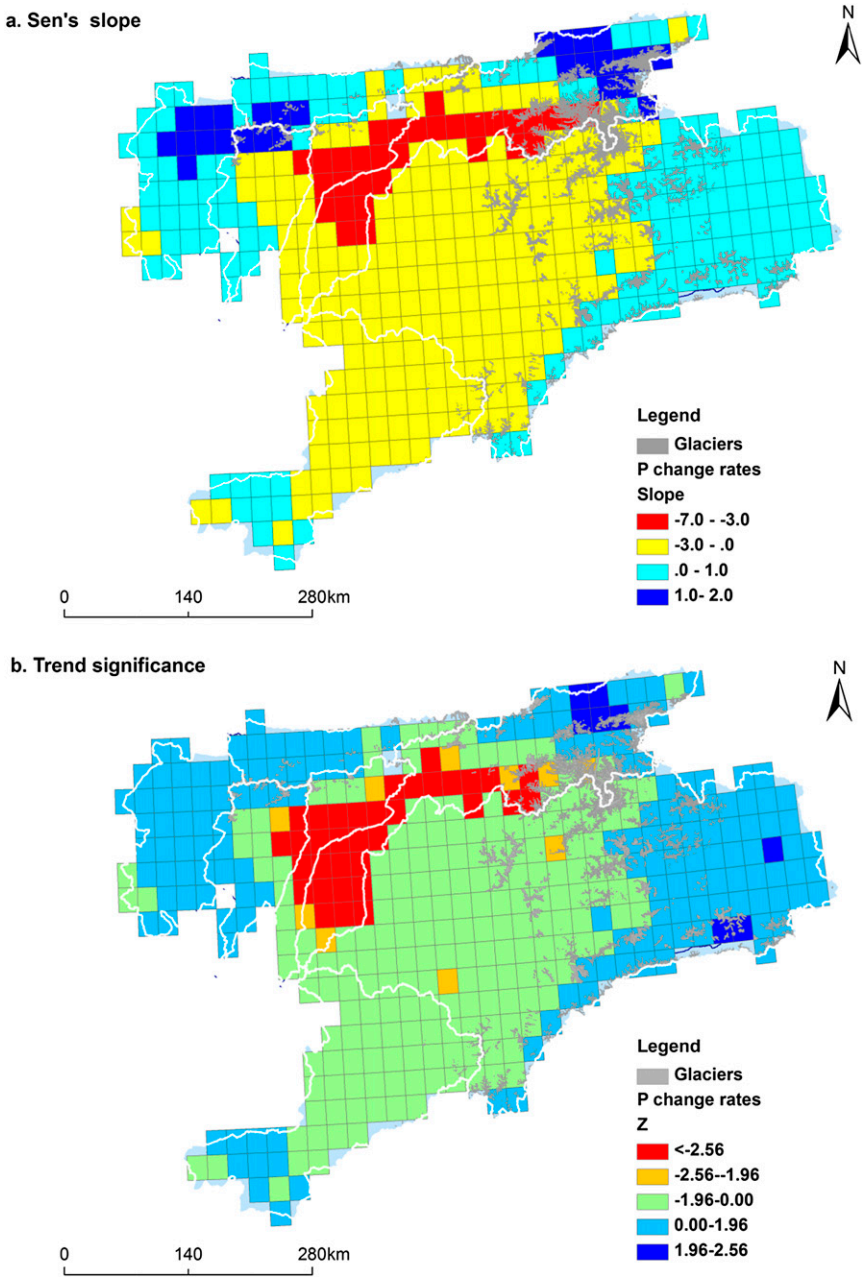

FIG. 2. Maps of the (a) rate of precipitation change and (b) trend significance of grid cells for APHRODITE data in the source region of the ADR in 1951–2007 in central Asia.

(2007), the R^2 suggests an acceptable consistency between the gridded data and the observation data. However, the slopes of the regression lines also suggest systematic bias between the gridded and observation data. The gridded data generally underestimate temperature and precipitation at high elevations, especially the latter. As each grid is treated as a meteorological station in the SWAT model, the lapse rates of temperature and precipitation are used to adjust the values at high elevations.

The initial temperature lapse rates (TLAPSs) are derived directly from PGMFD and observation data at the meteorological stations, which are then tuned during the model calibration with consideration for potential uncertainties involved in the gridded data. In this study, the PLAPSs were used to estimate precipitation at locations other than the observation sites. At low elevation, PLAPSs are determined by the combined use of APHRODITE and observation data at the meteorological

stations. At high elevation, precipitation is corrected by a mass accumulation–precipitation relation with the glacier. Kotlyakov and Krenke (1982) proposed an empirical formula that expresses this relation based on measurement data at 57 glacier stations around world. The relation is formulated as

$$A = 1.33(9.66 + T_s)^{2.85}, \quad (2)$$

where A is the ablation (or accumulation) at equilibrium line altitude (ELA) per year (mm) and T_s is the mean temperature in summer (June–August) at ELA (°C). For each glacier, the annual ablation at ELA was calculated via Eq. (2) over the period 1960–70, when glacier change in the study area was insignificant (Sorg et al. 2012). Precipitation was assumed as the ablation.

The gridded daily minimum and maximum temperature and precipitation and the tuned lapse rates are used to drive the simulation of the hydrological processes in the watershed.

2) Climate data series trend test

The Mann–Kendall test (Gilbert 1987; Hirsch et al. 1982, 1991) method is used for trend analysis of the temperature, precipitation, and discharge data series. The Mann–Kendall test is a nonparametric test, that is, it does not make any assumptions on the probability distribution of the underlying data and can address incomplete data series. The test rejects the null hypothesis if $Z \geq |Z_{cr}|$, where Z_{cr} is the critical value of the normal distribution at some Z confidence level. A positive Z value indicates an increasing trend and a negative Z indicates a decreasing trend. Sen's nonparametric method can give the slope and intercept of the linear trend line (Gilbert 1987; Sen 1968). Sen's slope is estimated as the median of $n(n-1)/2$ slopes of pairs of $(x_j : x_k)$ with $j > k$.

(i) Temperature

Based on the Mann–Kendall test, the mean temperature from PGMFD for 1951–2007 in the UADRB increased by 0.2°C decade^{-1}, the maximum temperature increased by 0.2°C decade^{-1}, and the minimum temperature increased by 0.3°C decade^{-1} (significant at $p < 0.01$). The rate of change in temperature derived from PGMFD is in phase with previous analyses [0.39°C by Hu et al. (2014); 0.31°–0.41°C by Giese et al. (2007); and 0.39°C by Chevallier et al. (2014)]. The variations in the exact magnitudes are due to the different temperature data sources, the time span of the statistics, and the statistical methods used in the studies.

(ii) Precipitation

The long-term trend of change in precipitation from AHPRODITE data for 1951–2007 is plotted in Fig. 2. For 1951–2007, precipitation for ~60% of the grid cells decreased, among which ~80% decreased significantly ($p < 0.05$). The rate of change varied between −7.0 and 0.0 mm decade^{-1}. Precipitation in not over 40% of the grid cells increased within the range of 0.0–2.0 mm decade^{-1}. In the study area, a comparison between observed precipitation from 29 meteorological stations and APHRODITE gridded precipitation at the corresponding grid cells shows 70% similar in trend of change.

On the basis of the Mann–Kendall test, temperature had an overall increasing trend and precipitation had an overall decreasing trend in 1951–2007, with few exceptions in the UADRB.

To assess the potential impact of observed climate change on water, Bouraoui et al. (2004) introduced a detrending approach for climatic variables based on trend analysis as follows:

$$T_0 = T - \beta_T(t_y - t_0) \quad \text{and} \quad (3)$$

$$P_0 = P - PP_m^{-1}\beta_P(t_y - t_0), \quad (4)$$

where T and P are actual data series of temperature and precipitation; T_0 and P_0 are detrended daily temperature and precipitation data series; P_m is monthly precipitation; β_T and β_P are the calculated Sen's slopes of linear trend lines of temperature and precipitation, respectively; t_0 is the base year; and the subscript y is the sequential number of years from the base year. If the calculated detrended precipitation is negative, it is set to the median value of observation series for that month.

In this study, the detrending method is used to assess the impact of observed changes in temperature and precipitation on streamflow and glacier melt. It is assumed that T_0 and P_0 denote climate without interference of climate change; then T and P are the actual climate with the so-called climate change fractions included as follows:

$$P = P_0 + dP \quad \text{and} \quad (5)$$

$$T = T_0 + dT. \quad (6)$$

3) Simulation scheme

To determine how the changes in temperature and/or precipitation affect glaciohydrological processes in the study area, the climatic forcing schemes are designated as in Table 2. Typically, scheme 4 (T_0, P_0) is treated as the background climatic conditions, and dT and dP are the changes in actual temperature and precipitation against the detrended values, respectively. A comparison of the simulation results may reveal how climate change affected the glaciohydrological processes during the given historical period. This is based on historical data and can support a

TABLE 2. Climate forcing schemes for the glacier-enhanced SWAT model simulation. The observed (T, P) is split into two components: $T = T_0 + dT$ and $P = P_0 + dP$. Then (dT, dP) is the climate change component.

Schemes	Temperature	Precipitation	Remark
Scheme 1	T	P	Observed climate variable
Scheme 2	T_0	P	Temperature change effect excluded
Scheme 3	T	P_0	Precipitation change effect excluded
Scheme 4	T_0	P_0	Climate change effect excluded

better understanding of future projections of the impacts of climate change in the study area.

3. Results and analyses

a. Model calibration and validation

The most sensitive parameters and the related scopes are covered in detail in similar other studies (Geza et al. 2009; Immerzeel et al. 2013; Luo et al. 2012, 2013; Lutz et al. 2013, 2014; Ragettli et al. 2013; Ryu et al. 2011). The calibration of these parameters in this study is performed by trial and error with respect to NSE, PBIAS, and R^2 for monthly streamflow at each hydrological station and glacier area changes. Acceptable calibration and validation results are obtained after repeated trials (Table 3). Glacier area change estimated by Konovalov and Shchetinnicov (1994) and Konovalov (2011) for the UADRB is used as reference value in tuning the parameters. The simulated and reported glacier area changes are compared for the tributary catchments of ADR (Fig. 3). A linear regression of the simulated and literature reported glacier area changes suggest 3% underestimation, with $R^2 = 0.85$. Therefore, the model performance in terms of the simulated glacier area change is acceptable.

The NSE and PBIAS evaluation indices for the calibration and validation processes are plotted in Fig. 4. For the calibration stage (Fig. 4a), NSE ≥ 0.74 suggests that the model performs "very good" or "good," based on the rating system by Moriasi et al. (2007). For the validation stage (Fig. 4b), the indices suggest very good model performance for 10 hydrological stations (NSE $>$ 0.75), good for four stations (NSE = 0.72–0.75), satisfactory for two stations (NSE = 0.62 and 0.64), and unsatisfactory for the Nurek station in VKRB (NSE = 0.33). Additionally, PBIAS suggests a very good model performance for most of the hydrological stations, except for Ninj Pyanj station in PYRB and Karatog station in SHRB. Nurek Dam was built in 1980, following which discharge at Nurek Station never returned to its natural state. Thus, the simulated natural discharge does not match the observed controlled discharge. Nevertheless, the PBIAS = −0.05% suggests that the simulated discharge is not significantly different from the actual discharge in terms of interannual water balance. Hydrographs of the observed and simulated monthly discharge at 17 hydrological stations (Fig. S3 in the supplemental material) also indicate that the simulated streamflow is reasonable.

b. Streamflow series trend analysis

The Mann–Kendall trend test results and Sen's slopes of the simulated annual streamflow series for 1951–2007 in the ADR and its seven primary tributaries are given in Table 4 and also plotted in Fig. 5. The streamflow showed a decreasing trend that was significant at $p < 0.05$ for PYRB, VKRB, and KFRB, but not significant at $p < 0.05$ for SHRB and KDRB. Conversely, the streamflow showed an increasing trend that was significant at $p < 0.05$ for KSRB, but not significant at $p < 0.05$ for ZVRB. The streamflow for the ADR, which is the sum of the seven primary tributaries,

TABLE 3. Most sensitive parameters and the final calibrated values or ranges for the glacier-enhanced SWAT model in the source region of the ADR in central Asia.

Sensitive parameters	Parameter definition	Parameter change range	Final parameter value range
TLAPS	Temperature lapse rate (°C km^{-1})	From −9 to −2	From −6.8 to −5.7
ALPHA_BF	Baseflow alpha factor	0–1	0.02–0.8
RCHRG_DP	Deep aquifer percolation factor	0–1	0.4
CH_K2	Channel effective hydraulic conductivity (mm h^{-1})	0–300	10–50
gmfmx	Degree-day factor for ice melt on 21 Jun (mm °C^{-1} day^{-1})	1.4–16.0	3.0–14.5
gmfmn	Degree-day factor for ice melt on 21 Dec (mm °C^{-1} day^{-1})	1.4–16.0	1.0–8.8
SMFMX	Degree-day factor for snowmelt on 21 Jun (mm °C^{-1} day^{-1})	1.4–6.7	2.5–3.5
SMFMN	Degree-day factor for snowmelt on 21 Dec (mm °C^{-1} day^{-1})	1.4–6.7	1.0–2.5

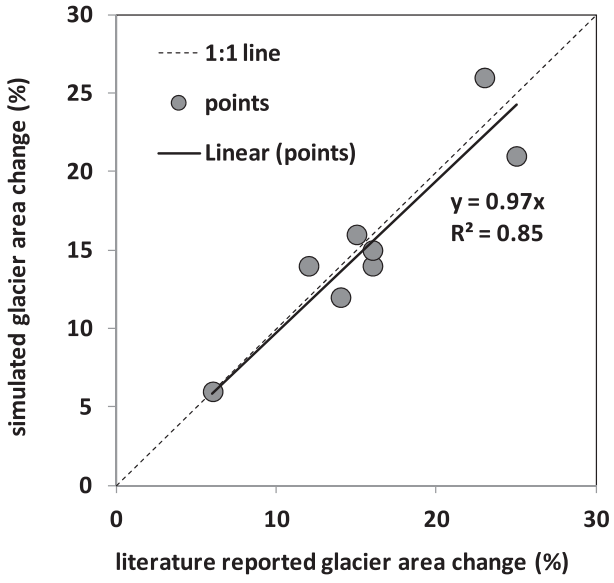

FIG. 3. Comparison of the rate of simulated glacier area shrinkage with that of literature value for tributary headwater catchments in the ADR basin in central Asia. The observed rate of shrinking of glaciers in 1960–80 is obtained from Konovalov and Shchetinnicov (1994) and the rate for 1960–2000 is obtained from Konovalov (2011).

tracked an overall decreasing trend that was significant at $p < 0.05$.

Based on the available observed streamflow data series, the results of the trend analysis and Sen's slopes of some tributaries are also compared in Fig. 5. Comparisons of the Sen's slopes and the intercepts of the linear trend lines between the simulated and observed series suggest that the simulation reproduces well the trend of change in PYRB, VKRB, and ZVRB. For KFRB and SHRB, the Sen's slopes for the simulated and observed series are similar, but the intercept of the former is larger than the latter, suggesting a systematic overestimation of the annual streamflow. The results of the Mann–Kendall trend test indicate that the trends in the simulated and observed series have different levels of significance. This discrepancy can be explained in terms of the different time spans of the statistics, as noted by Unger-Shayesteh et al. (2013). As also shown in Fig. S4, the slopes of the observed and simulated streamflow in PYRB and VKRB are significantly different for 1951–98 and 1951–2007.

The decreasing trend in streamflow in the ADR was further confirmed by Stulina and Eshchanov (2013) and also in the plots in Fig. 6. Stulina and Eshchanov (2013) compiled gauge streamflow records at Kerki gauge station (Fig. 1) and water withdrawal in the upper stream, which data are used here to evaluate the simulated total streamflow from the source regions of PYRB, ZVRB, KFRB, SHRB, and KDRB in the ADR (Fig. 6). The simulated and observed flows have very similar long-term trends of change. The comparison also suggests that the simulation reproduces the long-term trend of change with a larger intercept, indicating overestimation of the flow volume. The model overestimates annual flow at Kerki gauge station by 21%, which is the equivalent of 13.9 km^3. Zonn (2012) reported that, on average, 13.5 km^3 of water is annually diverted from the ADR via Karakum Canal to Ashgabat in Turkmenistan. The diversion engineering, established in the 1950s, is pivoted ~50 km above Kerki station. By excluding the water diversion to the Karakum Canal, the difference between the simulated and observed water flow at Kerki station is minor.

c. *Attribution of runoff changes*

1) TEMPERATURE CHANGE

Compared with the detrended scenarios, temperature changes in the tributary catchments are presented in Table 5. Surprisingly, the most significant temperature increase during 1951–2007 was in PYRB and VKRB, which have the highest average elevation among the seven tributary catchments. Temperature in KDRB was almost stable. While minimum temperature rose in all of the tributary basins, maximum temperature rose at a much smaller magnitude or even fell, although very slightly.

Seasonally, temperature increased throughout the year. Based on the Mann–Kendall trend test, the trend of increase was significant for some months and insignificant for others. Temperature increase was higher in the cold season than in the warm season (Fig. 7a), as noted by other previous studies (Siegfried et al. 2012; Unger-Shayesteh et al. 2013). The increase in mean annual temperature was primarily induced by the increase in minimum temperature (Unger-Shayesteh et al. 2013).

2) PRECIPITATION CHANGE

For 1951–2007, precipitation in the UADRB decreased significantly (Table 5). Based on the detrending analysis, precipitation in the UADRB decreased by 10.8%, and a remarkable spatial heterogeneity was found for the precipitation change. The precipitation declined by almost 15% over the nearly 50-yr period in PYRB, doubling the decline in VKRB, KFRB, and KDRB. However, it slightly increased in ZVRB and KSRB. Seasonally, precipitation primarily dropped during February–May (Fig. 7b).

3) CONTRIBUTOR OF STREAMFLOW CHANGE

Average annual flow in the UADRB was 72.6 km^3, with a maximum of 123.6 km^3 in 1969 and a minimum of

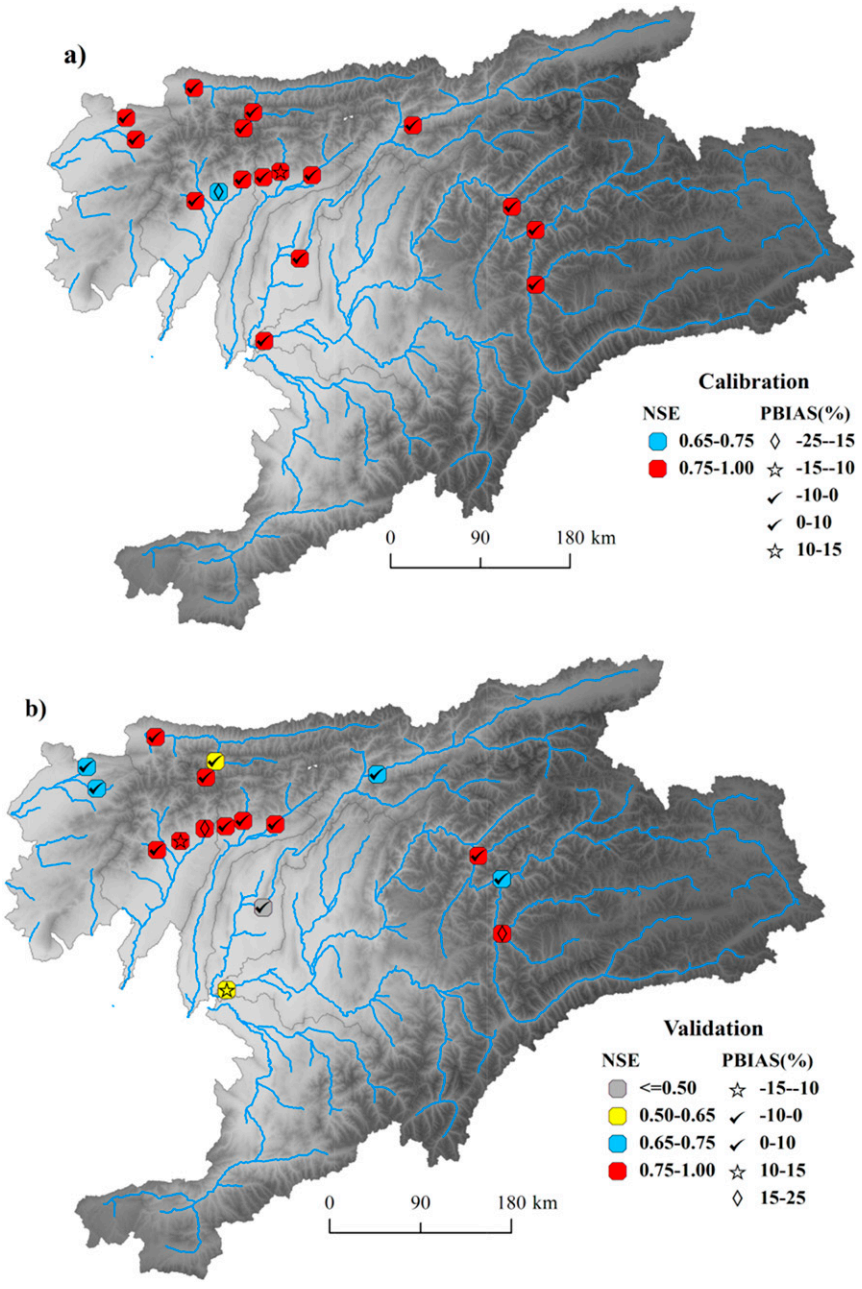

FIG. 4. NSE and PBIAS of simulated monthly runoff for the (a) calibration and (b) validation periods using 17 hydrological stations in the ADR basin in central Asia.

42.4 km^3 in 2006 (Table 6). The PYRB and VKRB (with flow volumes of 32.9 and 17.7 km^3, respectively) are the most glacierized among the seven main tributaries of ADR, together contributing 70% to total flow in the UADRB. The trend of streamflow in the ADR decreased significantly ($p < 0.05$) during 1951–2007, but with some variations among the tributaries, as described in the previous section. The simulated streamflow forced by different climatic input schemes reveals the primary factor driving the decrease in streamflow in the ADR. Table 6 shows the results of the mean annual flow volumes in the ADR and its primary tributaries under different climatic schemes for 1951–2007. The statistics suggest that change in precipitation, other than that in temperature, was the dominant cause of the change in streamflow in both the tributaries and the mainstream. For the UADRB, streamflow decreased by 15.5% due to decrease in precipitation, but only increased by 0.2%

TABLE 4. Mann–Kendall trend test results for ice melt, glacier melt, and annual discharge in the ADR and its tributaries in central Asia. Slope and Z are parameters of the Mann–Kendall test. Trends: a = decrease but insignificant at $p < 0.05$; b = decrease but significant at $p < 0.05$; c = increase but insignificant at $p < 0.05$; and d = increase but significant at $p < 0.05$.

Variables index	PYRB	VKRB	ZVRB	KFRB	SHRB	KSRB	KDRB	UADRB
1951–2007								
Ice melt								
Z	−0.6	−1.2	−1.3	−6.4	−2.7	−3.2	−4.6	−0.9
Slope (mm yr^{-1})	−0.04	−0.11	−0.09	−0.25	−0.08	−0.01	−0.03	−0.06
Intercept (mm)	96.2	259.5	209.1	509.6	171.7	28.2	59.4	136.0
Trend	*a*	*a*	*a*	*b*	*b*	*b*	*b*	*a*
Glacier melt								
Z	−2.9	−3.2	−4.9	−7.4	−5.0	−6.1	−7.2	−3.4
Slope (mm yr^{-1})	−0.2	−0.37	−0.39	−0.37	−0.18	−0.03	0.05	−0.21
Intercept (mm)	443.5	833.9	833.4	765.3	382.0	52.9	103.8	463.4
Trend	*b*	*b*	*b*	*b*	*b*	*b*	*b*	*b*
Discharge								
Z	−3.5	−2.9	0.1	−2.5	−0.5	2.3	−1.5	−3.1
Slope (m^3 s^{-1} yr^{-1})	−6.5	−2.35	0.02	−0.96	−0.07	0.33	−0.89	−11.25
Intercept (m^3 s^{-1})	13908.0	5202.3	115.4	2085.7	218.0	−587.4	1989.8	24611.3
Trend	*b*	*b*	*c*	*b*	*a*	*d*	*a*	*b*
1951–90								
Ice melt								
Z	0.4	−0.5	0.1	−3.1	−0.1	−2.1	−1.5	0.2
Slope (mm yr^{-1})	0.05	−0.08	0.01	−0.21	−0.01	−0.02	−0.01	0.02
Intercept (mm)	−72.3	203.3	23.0	428.7	24.5	34.1	29.9	−20.6
Trend	*c*	*a*	*c*	*d*	*a*	*b*	*a*	*c*
Glacier melt								
Z	−0.7	−0.9	−2.0	−3.8	−1.7	−3.9	−4.4	−0.9
Slope (mm yr^{-1})	−0.1	−0.18	−0.26	−0.29	−0.09	−0.03	−0.05	−0.12
Intercept (mm)	244.0	453.0	574.9	599.1	198.7	55.2	94.5	280.0
Trend	*a*	*a*	*b*	*b*	*a*	*b*	*b*	*a*
Discharge								
Z	−1.8	0.5	1.6	0.9	1.4	2.3	−2.8	−1.4
Slope (m^3 s^{-1} yr^{-1})	−4.39	0.45	0.46	0.55	0.26	0.41	−2.76	−6.25
Intercept (m^3 s^{-1})	9737.8	−285.6	−758.0	−887.9	−424.5	−749.8	5669.6	14718.8
Trend	*a*	*c*	*c*	*c*	*c*	*d*	*b*	*a*

as a result of increase in temperature. In all the tributaries, change in precipitation was still the dominant factor for the change in streamflow. Among the tributaries, PYRB ranked the highest in terms of streamflow decline (22.4%), relative to the detrended input scheme (T_0, P_0). This is due mainly to the fall in precipitation rather than the rise in temperature. Streamflow in ZVRB and KSRB only increased by 2.0% and 2.3%, respectively, due to increase in precipitation in the catchments, which was still larger than the change due to increase in temperature (Table 6).

Seasonally, the most significant change in streamflow was in spring, followed by that in summer (Fig. 8). The decrease in streamflow in spring and summer was 72%–88% higher than that in autumn and winter in PYRB, VKRB, KFRB, and SHRB. Also, the streamflow increase in spring and summer was 72% higher than that in the other seasons in ZVRB. Streamflow in PYRB and KFRB decreased most (about 43 mm in spring and 20–30 mm in summer) because of climate change, especially the decrease in precipitation, which was mainly in February–May.

Although different tributaries depict different long-term trends of change in annual streamflow (either increase or decrease or statistically significant or not), PYRB, VKRB, SHRB, KDRB, and KFRB dominate the long-term pattern of change in the ADR. This is because these basins account for 91% of total streamflow in the ADR (Table 6). Thus, the trend of streamflow in the ADR is similar to that in the main tributaries, as affected mainly by the changes in precipitation.

4. Discussion

In the ADR, the high mountain regions are covered by large areas of glaciers, and glacier melt is an important source of water for the river systems in the region. Glacier melt is the sum of runoff generated from

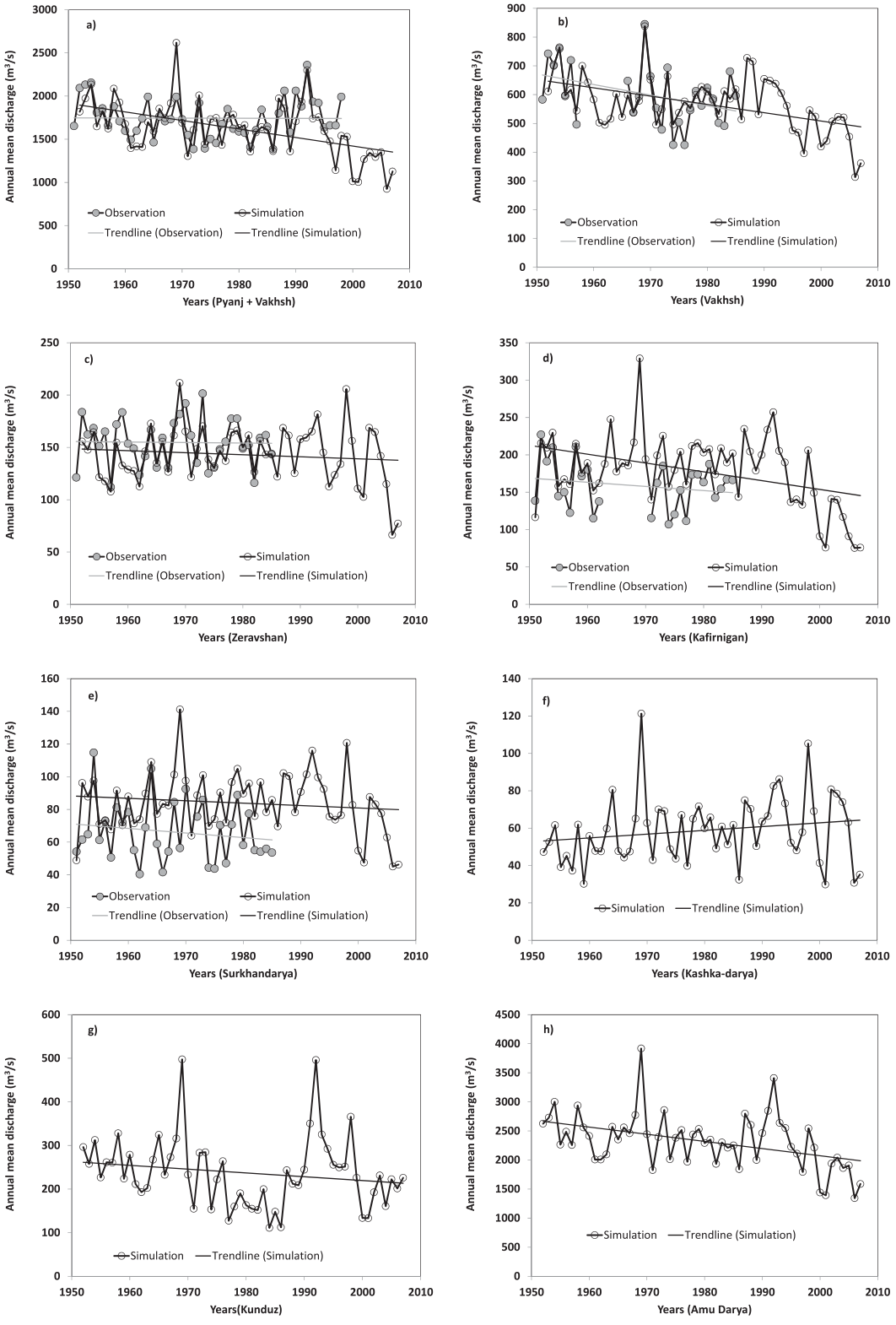

FIG. 5. Trend in simulated streamflow in the ADR and its tributaries and a comparison of simulated and observed trends of streamflow in Pyanj, Vakhsh, Zeravshan, Kafirnigan, and Surkhandarya River basins: (a) observed flow data are adapted from Stulina and Eshchanov (2013) and (b)–(e) data are adapted from IHP (1999).

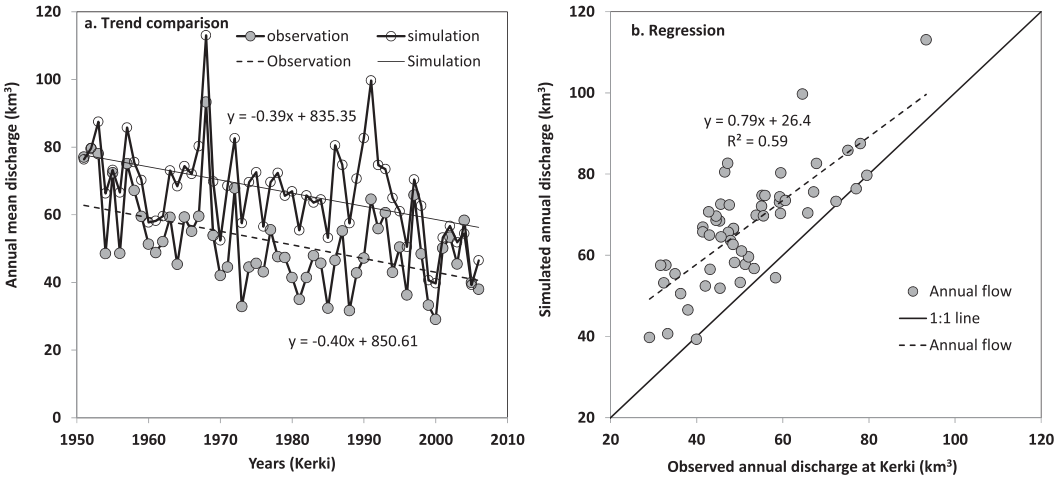

FIG. 6. Comparison of simulated and observed streamflow in the ADR in 1951–2007 in central Asia. The observed data are adapted from Stulina and Eshchanov (2013), and the simulated flow is for Pyanj, Vakhsh, Kafirnigan, Surkhandarya, and Kunduz Rivers.

supraglacial snowmelt, rainfall–runoff over glaciers, and ice melt. Ice melt leads to a loss of glaciers, which store precipitation over the years and release it with delayed effect to feed streamflow. It is a critical input term of the water balance components after precipitation. As such, it is important to determine the change in ice melt and whether the change is also the main cause of streamflow decline in the headwater regions of the ADR basin in 1951–2007.

For 1951–2007, the trend in ice melt in all of the glacierized catchments decreased. However, the trend of the decline was not significant ($p < 0.05$) for the more heavily glacierized catchments (PYRB and VKRB). Conversely, the trend of the decline was significant ($p < 0.05$) in the less glacierized catchments in the ADR (Table 4).

As ice melt in summer (June–August) accounts for 94%, 81%, 76%, 84%, 96%, 86%, and 94% of the annual value in PYRB, VKRB, ZVRB, KFRB, SHRB, KSRB, and KDRB, respectively, the subsequent discussion is focused on ice melt during that period. The ice melt offsets due to temperature rise, change in precipitation, and the combined effects are plotted in Fig. 9. The plots are based on simulation forcing by different temperature and precipitation scenarios as described before.

Generally, annual average ice melt increased because of the excessive compensation by the warming temperature in 1951–2007 (Table 5). Ice melt increased by 7.7%, 10.2%, 9.0%, and 0.2% due to temperature rise in summer (Fig. 9) in PYRB, VKRB, ZVRB, and KFRB, respectively. The offset by ice melt due to precipitation was generally small, except for KFRB. However, this process is generally complex and diverse in the different catchments.

On the one hand, precipitation change affects ice melt via change in supraglacial snow. For example, decreasing precipitation could result in less snow cover over

TABLE 5. Average change in annual temperature and annual precipitation in 1951–2007 in the source regions of the ADR and its primary tributaries in central Asia. Change in temperature is expressed as the average of the trend terms over the given period. Change in precipitation is expressed as the change in the trend term average relative to the detrended term average over the given period. Note that ΔT is change in average annual temperature; ΔT_{min} is change in minimum annual temperature; ΔT_{max} is change in maximum annual temperature; and ΔP is percent change in the annual precipitation. All the changes are significant at $p < 0.05$.

Variable	UADRB	PYRB	VKRB	ZVRB	KFRB	SHRB	KSRB	KDRB
Annual change								
ΔT (°C)	0.41	0.48	0.63	0.33	0.30	0.19	0.28	0.07
ΔT_{max} (°C)	0.19	0.22	0.38	0.13	0.15	0.05	0.06	−0.04
ΔT_{min} (°C)	0.63	0.74	0.88	0.52	0.44	0.33	0.49	0.18
ΔP (%)	−10.8	−14.5	−7.5	1.2	−7.9	−2.9	1.0	−7.7
Change in glacier melt season								
ΔT (°C)	0.20	0.26	0.32	0.22	0.17	0.23	0.33	0.03
ΔT_{max} (°C)	0.03	0.04	0.06	0.06	0.01	0.08	0.20	−0.09
ΔT_{min} (°C)	0.42	0.47	0.57	0.38	0.32	0.38	0.46	0.14
ΔP (%)	−2.2	19.1	−1.2	−9.3	−3.8	−1.2	0.0	44.7

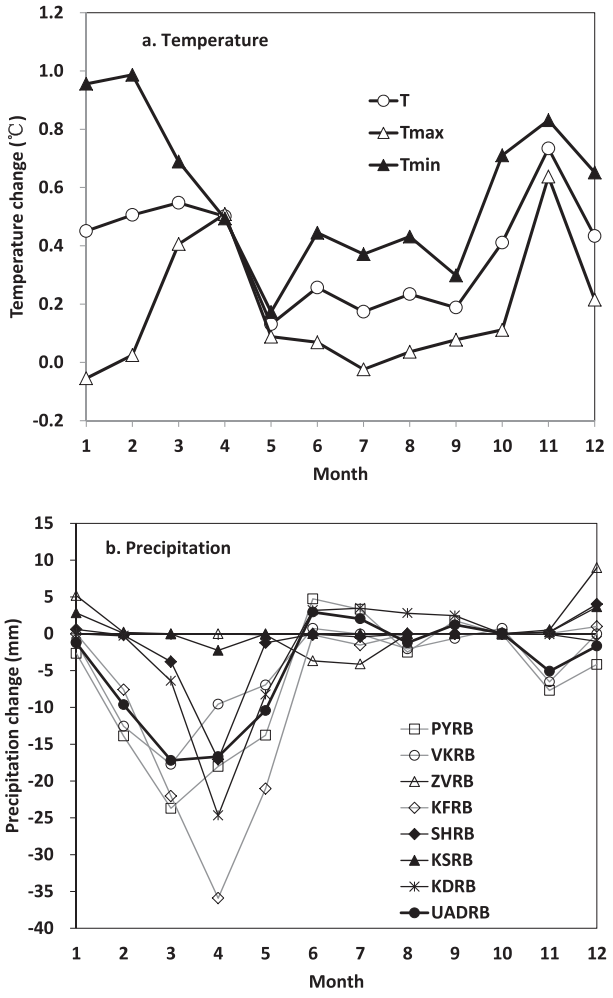

FIG. 7. Changes in monthly (a) temperature and (b) precipitation in the source region of the ADR in central Asia; T, T_{max}, and T_{min} are the mean, maximum, and minimum monthly temperatures, respectively. The temperature data are from PGMFD and precipitation data are from the APHRODITE database.

glaciers and more exposure of ice, resulting in more ice melt, especially under warming temperatures. On the other hand, precipitation change could affect mass accumulation and thus the area of ablation zone of glaciers. Ice melt slightly increased in both ZVRB and SHRB catchments because of the change in precipitation in 1951–2007. Precipitation grid cells located in glacierized areas in the two catchments mostly had increasing trends, especially for the SHRB (Fig. 2). Moreover, the increase was mainly in winter, with a small decrease in summer (Fig. 7b). Also in the basins, about 40% of the precipitation fell in winter and another 40% in spring. The increase in snowfall due to increase in precipitation during winter months offsets the decline in snowfall in summer. Thus, the glaciers advanced because of increased mass accumulation, as reported by Kapnick et al. (2014) in the discussion of the "Karakoram anomaly" of glacier changes in the last few decades. Mass accumulation increased and glacier area expanded in 1951–2007 under the temperature and precipitation forcing scenario (T_0, $P_0 + dP$) in relation to the (T_0, P_0) scenario (Fig. 10). Glacier area in SHRB increased even faster than in ZVRB provided that the impact of temperature rise was neglected (Fig. 10). On the one hand, the increase in ice melt was due to the decrease in supraglacial snow cover, which was in turn caused by the decline in precipitation during the melt season (Table 5). Based on the degree-day factor approach, ice melt is theoretically the product of the ice melt degree-day factor and melt zone area. On the other hand, ice melt increased because of expanding glacier area and stable melt rate with constant temperature. Annually, the slight increase in ice melt still could not offset the increase in accumulation; thus, an increasing glacier area appeared under the (T_0, $P_0 + dP$) scenario.

In PYRB, VKRB, and especially in KFRB, the offset by ice melt due to change in precipitation was negative (Fig. 9). In these catchments, annual precipitation decreased by 7.5%–14.5% (Table 5). Precipitation grid cells covering over 60% of glacier areas in PYRB and VKRB and nearly all in KFRB implied decreasing trends (Fig. 2). Moreover, the decrease in precipitation was mainly in winter and spring (Fig. 7b), possibly resulting in a negative mass balance. In comparing the change in glacier area under the (T_0, $P_0 + dP$) and (T_0, P_0) climate schemes, the effect of the component of climate change due to temperature on glacier area change is excluded. Under this treatment, glacier area in the three catchments continued to decrease (Fig. 10). The decrease can be partially explained in terms of the lower input (of precipitation) to the glacier during the accumulation season. The decrease in precipitation under constant temperature resulted in negative mass balance and retreat of glacier area. Thus, based on the degree-day factor analysis, the intensity of ice melt remained unchanged and the ice melt volume subsequently decreased. More decrease in precipitation in the glacierized areas of KFRB (Figs. 2, 7b) caused a rapid glacier retreat, with an area reduction of ~25%. In the other two catchments, the area shrunk by less than 5% (Fig. 10). This may explain why the offset in ice melt reduction was a bit quite larger in KFRB than in the other two catchments.

In addition to ice melt, glacier melt involves supraglacial snowmelt and direct rainfall runoff, which are critical for the changes in precipitation. The trend in glacier melt decreased significantly ($p < 0.05$) in all the glacier-prone catchments in 1951–2007. The negativity of the slope of glacier melt was higher than that of ice

TABLE 6. Mean annual streamflow based on a simulation from 1951 to 2007 forced by different climatic change schemes for the ADR basin in central Asia. Scheme ($T_0 + dT$, $P_0 + dP$) is the observed temperature and precipitation, (T_0, P_0) is the detrended temperature and precipitation, and dT and dP are the detrended terms for the temperature and precipitation data series, respectively.

	Annual flow volume (km^3)							Relative change to scheme 4 (%)		
	Scheme 1 ($T_0 + dT$, $P_0 + dP$)				Scheme 2	Scheme 3	Scheme 4			
	Mean	Max	Min	Std dev	(T_0, $P_0 + dP$) mean	($T_0 + dT$, P_0) mean	(T_0, P_0) mean	$dT + dP$	dT	dP
PYRB	32.9	56.1	17.8	7.4	32.8	42.5	42.4	−22.4	0.3	−22.7
VKRB	17.7	26.4	9.9	2.9	17.6	19.4	19.3	−8.5	0.3	−8.8
KFRB	5.6	10.4	2.4	1.5	5.6	6.3	6.3	−11.6	0.0	−11.6
SHRB	2.7	4.5	1.4	0.6	2.7	2.8	2.8	−3.7	−0.1	−3.7
ZVRB	4.5	6.7	2.1	0.9	4.5	4.4	4.4	2.6	0.6	2.0
KSRB	1.9	3.8	0.9	0.6	1.9	1.8	1.8	1.5	−0.8	2.3
KDRB	7.4	15.7	3.5	2.6	7.4	8.7	8.7	−15.1	0.1	−15.2
UADRB	72.6	123.6	42.4	14.6	72.4	85.9	85.7	−15.3	0.2	−15.5

melt (Table 4). This was clearly related to the reduction in supraglacial snowmelt and rainfall–runoff over ice due to decreasing precipitation.

Both ice melt and glacier melt declined in 1951–2007 in the tributary catchments and the entire UADRB. The decline in ice melt was primarily due to the intrinsic negative equilibrium of the glaciers. Although warming temperature increased ice melt in most glacierized catchments, the increase failed to reverse the decline in long-term run. The decline in glacier melt was higher than that in ice melt, which was primarily attributed to the decreasing precipitation. It is good to note that precipitation change is critical in the discussion of glacier melt change under climate change conditions.

For the glacierized subbasins or HRUs, increase in ice melt due to warming temperature or decreasing ice melt primarily attributed to glacier area shrinkage could change the trend in runoff. In relating this to the entire headwater regions of the ADR basin, ice melt increased by 1.85 mm and streamflow by 1.03 mm if there is only an increase in temperature for 1951–2007 [as suggested by comparison of the ($T_0 + dT$, P_0) and (T_0, P_0) schemes]. If only precipitation decreased [as suggested by comparison of the (T_0, $P_0 + dP$) and (T_0, P_0) schemes], ice melt decreased by 0.2 mm and streamflow by 59.1 mm. It is therefore deduced that the role of increase in ice melt due to warming temperature is minimal. This could be because ice melt contributed only 8.7%, 8.5%, 7.1%, 2.9%, 2.4%, 0.7%, and 0.9% to streamflow in PYRB, VKRB, ZVRB, KFRB, SHRB, KSRB, and KDRB, respectively. Because of the small contribution of ice

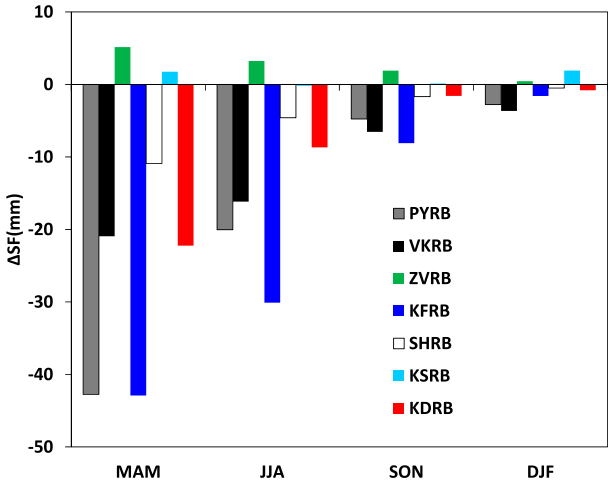

FIG. 8. Seasonal offset [March–May (MAM), June–August (JJA), September–November (SON), and December–February (DJF)] of tributary streamflow due to change in precipitation and temperature in 1951–2007 in the ADR basin in central Asia. Streamflow offset (ΔSF) is under observed climate scenario relative to detrended climate scenario.

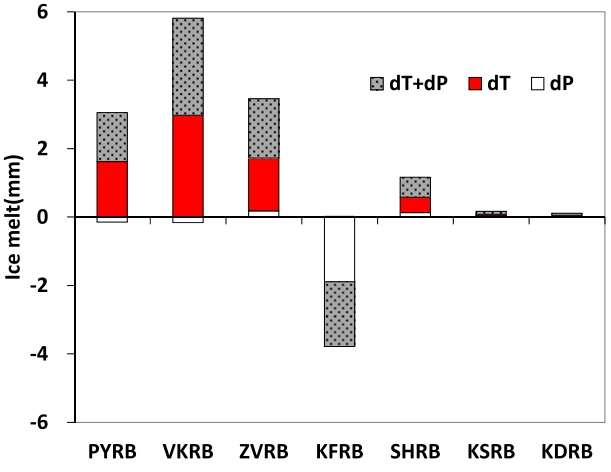

FIG. 9. Change in ice melt during JJA due to change in temperature, precipitation, and the combined effects in 1951–2007 in the tributary source regions of the ADR in central Asia.

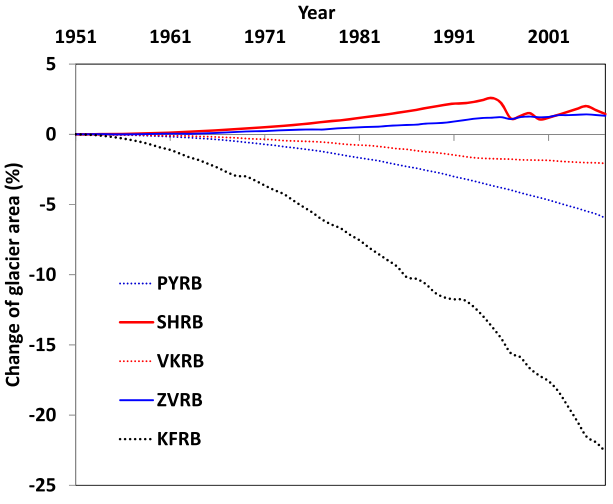

FIG. 10. Change in glacier area under the (T_0, P_0 + dP) climate scenario relative to the (T_0, P_0) scenario in 1951–2007 in the tributary source regions of the ADR in central Asia.

melt to streamflow, the interannual compensation and seasonal regulation functions of ice melt over streamflow were unapparent in the UADRB. Instead, the decrease in precipitation was still the dominant driver of runoff decline in the region. It is, however, good to note that this finding does not necessarily suggest a worsening trend in water availability in the ADR basin. If precipitation increases or even stabilizes in the future, there might be an increase in the streamflow. Hence, this does not in any way imply that in some glacierized central Asian catchments, the days of abundant water could soon be over because of glacier loss, as projected by Sorg et al. (2014).

5. Conclusions

In this study, APHRODITE precipitation and the PGMFD temperature grid database were used to force the distributed, glacier-enhanced SWAT model to simulate glaciohydrological processes in the UADRB in central Asia for 1951–2007. The simulation revealed the main factors of long-term streamflow change in the region.

It is, however, important to note that, because of scarce ground data availability, evaluations based on gridded APHRODITE precipitation data for the high mountain area only provide the basis for reference. The glacier–precipitation relation is useful in estimating precipitation lapse rates in high-elevation areas of the glacierized catchments. Meanwhile, the differences between the simulated and observed streamflow in the ADR point to uncertainties in the precipitation data and other areas of the simulation process in the high mountain region.

Warming temperature is a critical element of the changes in ice/glacier melt. The glacier-enhanced SWAT model successfully identified the reasons for the changes in ice/glacier melt in the UADRB. The decreasing in ice melt was primarily attributed to glacier area shrinkage. However, the results show that the changes in glacier melt were dominantly driven by the changes in precipitation.

Annual streamflow in the UADRB was estimated at 72.6 km^3, showing a declining trend for 1951–2007. The change in precipitation was the dominant reason for the change in streamflow in the tributaries and the mainstream of the ADR. Streamflow decreased by 15.5% in the UADRB because of a decrease in precipitation, but only increased by 0.2% because of warming temperatures. The most significant reduction in streamflow was in the PYRB, and the decrease in precipitation surpassed the increase in temperature, resulting in reduced streamflow. However, it was the increase in precipitation that was driving the increase in streamflow in ZVRB and KSRB. Although the long-term trends of change in streamflow in the tributaries were diverse, overall streamflow in the ADR decreased in 1951–2007. The decrease in streamflow calls for the implementation of tighter water use policies in the downstream region. This is particularly critical in the face of the intense disputes over transboundary river water use and the projected increase in water demand due to the growing population in the region.

Acknowledgments. This study is funded by the Natural Science Foundation of China (Grant 41130641) and the Ministry of Science and Technology of China (Grant 2010DFA92720 and 2012BAC19B07).

REFERENCES

Agal'tseva, N., M. Bolgov, T. Y. Spektorman, M. Trubetskova, and V. Chub, 2011: Estimating hydrological characteristics in the Amu Darya River basin under climate change conditions. *Russ. Meteor. Hydrol.*, **36**, 681–689, doi:10.3103/S1068373911100062.

Aizen, V. B., E. M. Aizen, J. M. Melack, and J. Dozier, 1997: Climatic and hydrologic changes in the Tien Shan, central Asia. *J. Climate*, **10**, 1393–1404, doi:10.1175/1520-0442(1997)010<1393:CAHCIT>2.0.CO;2.

Arnold, J. G., and Coauthors, 2012: SWAT: Model use, calibration, and validation. *Trans. ASABE*, **55**, 1491–1508, doi:10.13031/2013.42256.

Bahr, D. B., W. T. Pfeffer, and G. Kaser, 2015: A review of volume-area scaling of glaciers. *Rev. Geophys.*, **53**, 95–140, doi:10.1002/2014RG000470.

Barnett, T. P., J. C. Adam, and D. P. Lettenmaier, 2005: Potential impacts of a warming climate on water availability in snow-dominated regions. *Nature*, **438**, 303–309, doi:10.1038/nature04141.

Bouraoui, F., B. Grizzetti, K. Granlund, S. Rekolainen, and G. Bidoglio, 2004: Impact of climate change on the water cycle

and nutrient losses in a Finnish catchment. *Climatic Change*, **66**, 109–126, doi:10.1023/B:CLIM.0000043147.09365.e3.

Chen, J., and A. Ohmura, 1990: Estimation of alpine glacier water resources and their change since the 1870s. *IAHS Publ.*, **193**, 127–135.

Chevallier, P., B. Pouyaud, M. Mojaisky, M. Bolgov, O. Olsson, M. Bauer, and J. Froebrich, 2014: River flow regime and snow cover of the Pamir Alay (central Asia) in a changing climate. *Hydrol. Sci. J.*, **59**, 1491–1506, doi:10.1080/02626667.2013.838004.

Froebrich, J., and O. Kayumov, 2004: Water management aspects of Amu Darya. *Dying and Dead Seas: Climatic Versus Anthropic Causes*, J. J. Nihoul, P. Zavialov, and P. Micklin, Eds., Springer, 49–76.

Gan, R., Y. Luo, Q. Zuo, and L. Sun, 2015: Effects of projected climate change on the glacier and runoff generation in the Naryn River basin, central Asia. *J. Hydrol.*, **523**, 240–251, doi:10.1016/j.jhydrol.2015.01.057.

Gassman, P. W., M. R. Reyes, C. H. Green, and J. G. Arnold, 2007: The soil and water assessment tool: Historical development, applications, and future research directions. *Trans. ASABE*, **50**, 1211–1250, doi:10.13031/2013.23637.

Geza, M., E. P. Poeter, and J. E. McCray, 2009: Quantifying predictive uncertainty for a mountain-watershed model. *J. Hydrol.*, **376**, 170–181, doi:10.1016/j.jhydrol.2009.07.025.

Giese, E., I. Mossig, D. Rybski, and A. Bunde, 2007: Long-term analysis of air temperature trends in central Asia. *Erdkunde*, **61**, 186–202, doi:10.3112/erdkunde.2007.02.05.

Gilbert, R. O., 1987: *Statistical Methods for Environmental Pollution Monitoring*. John Wiley & Sons, 320 pp.

Hagg, W., L. N. Braun, M. Kuhn, and T. I. Nesgaard, 2007: Modelling of hydrological response to climate change in glacierized central Asian catchments. *J. Hydrol.*, **332**, 40–53, doi:10.1016/j.jhydrol.2006.06.021.

——, M. Hoelzle, S. Wagner, E. Mayr, and Z. Klose, 2013: Glacier and runoff changes in the Rukhk catchment, upper Amu-Darya basin until 2050. *Global Planet. Change*, **110**, 62–73, doi:10.1016/j.gloplacha.2013.05.005.

Hirsch, R. M., J. R. Slack, and R. A. Smith, 1982: Techniques of trend analysis for monthly water quality data. *Water Resour. Res.*, **18**, 107–121, doi:10.1029/WR018i001p00107.

——, R. B. Alexander, and R. A. Smith, 1991: Selection of methods for the detection and estimation of trends in water quality. *Water Resour. Res.*, **27**, 803–813, doi:10.1029/91WR00259.

Hu, Z. Y., C. Zhang, Q. Hu, and H. Q. Tian, 2014: Temperature changes in central Asia from 1979 to 2011 based on multiple datasets. *J. Climate*, **27**, 1143–1167, doi:10.1175/JCLI-D-13-00064.1.

IHP, 1999: World water resources and their use: A joint SHI/UNESCO product. International Hydrological Programme, accessed 1 October 2013. [Available online at http://hydrologie.org/DON/html/.]

Immerzeel, W. W., L. P. H. van Beek, and M. F. P. Bierkens, 2010: Climate change will affect the Asian water towers. *Science*, **328**, 1382–1385, doi:10.1126/science.1183188.

——, ——, M. Konz, A. B. Shrestha, and M. F. P. Bierkens, 2012: Hydrological response to climate change in a glacierized catchment in the Himalayas. *Climatic Change*, **110**, 721–736, doi:10.1007/s10584-011-0143-4.

——, F. Pellicciotti, and M. F. P. Bierkens, 2013: Rising river flows throughout the twenty-first century in two Himalayan glacierized watersheds. *Nat. Geosci.*, **6**, 742–745, doi:10.1038/ngeo1896.

Kapnick, S. B., T. L. Delworth, M. Ashfaq, S. Malyshev, and P. C. D. Milly, 2014: Snowfall less sensitive to warming in Karakoram than in Himalayas due to a unique seasonal cycle. *Nat. Geosci.*, **7**, 834–840, doi:10.1038/ngeo2269.

Konovalov, V. G., 2011: Past and prospective changes in the state of central Asian glaciers. *Ice Snow*, **3** (115), 1–15.

——, and A. S. Shchetinnicov, 1994: Evolution of glaciation in the Pamiro–Alai Mountains and its effect on river run-off. *J. Glaciol.*, **40** (134), 149–157.

Kotlyakov, V. M., and A. N. Krenke, 1982: Investigations of the hydrological conditions of alpine regions by glaciological methods. *IAHS Publ.*, **138**, 31–42.

Kure, S., S. Jang, N. Ohara, M. L. Kavvas, and Z. Q. Chen, 2013: Hydrologic impact of regional climate change for the snowfed and glacierfed river basins in the Republic of Tajikistan: Hydrological response of flow to climate change. *Hydrol. Processes*, **27**, 4057–4070, doi:10.1002/hyp.9535.

Li, L. H., M. Shang, M. S. Zhang, S. Ahmad, and Y. Huang, 2014: Snowmelt runoff simulation driven by APHRODITE precipitation dataset. *Shuikexue Jinzhan*, **25** (1), 53–59.

Liu, S. Y., W. X. Sun, and Y. P. Shen, 2003: Glacier change since the little ice age maximum in the western Qilian Mountains, northwest China. *J. Glaciol.*, **49**, 117–124, doi:10.3189/172756503781830926.

Luo, Y., J. Arnold, P. Allen, and X. Chen, 2012: Baseflow simulation using SWAT model in an inland river basin in Tianshan Mountains, northwest China. *Hydrol. Earth Syst. Sci.*, **16**, doi:10.5194/hess-16-1259-2012.

——, ——, S. Liu, X. Wang, and X. Chen, 2013: Inclusion of glacier processes for distributed hydrological modeling at basin scale with application to a watershed in Tianshan Mountains, northwest China. *J. Hydrol.*, **477**, 72–85, doi:10.1016/j.jhydrol.2012.11.005.

Lutz, A. F., W. W. Immerzeel, A. Gobiet, F. Pellicciotti, and M. F. P. Bierkens, 2013: Comparison of climate change signals in CMIP3 and CMIP5 multi-model ensembles and implications for central Asian glaciers. *Hydrol. Earth Syst. Sci.*, **17**, 3661–3677, doi:10.5194/hess-17-3661-2013.

——, ——, A. B. Shrestha, and M. F. P. Bierkens, 2014: Consistent increase in High Asia's runoff due to increasing glacier melt and precipitation. *Nat. Climate Change*, **4**, 587–592, doi:10.1038/nclimate2237.

Ma, C., L. Sun, S. Liu, M. a. Shao, and Y. Luo, 2015: Impact of climate change on the streamflow in the glacierized Chu River basin, central Asia. *J. Arid Land*, **7**, 501–513, doi:10.1007/s40333-015-0041-0.

Moriasi, D., J. Arnold, M. Van Liew, R. Bingner, R. Harmel, and T. Veith, 2007: Model evaluation guidelines for systematic quantification of accuracy in watershed simulations. *Trans. ASABE*, **50**, 885–900, doi:10.13031/2013.23153.

Neitsch, S. L., J. G. Arnold, J. R. Kiniry, and J. R. Williams, 2011: Soil and water assessment tool theoretical documentation, version 2009. Rep. TR-406, Texas Water Resources Institute, 618 pp.

Nezlin, N. P., A. G. Kostianoy, and S. A. Lebedev, 2004: Interannual variations of the discharge of Amu Darya and Syr Darya estimated from global atmospheric precipitation. *J. Mar. Syst.*, **47**, 67–75, doi:10.1016/j.jmarsys.2003.12.009.

Olsson, O., M. Gassmann, K. Wegerich, and M. Bauer, 2010: Identification of the effective water availability from streamflows in the Zerafshan River basin, central Asia. *J. Hydrol.*, **390**, 190–197, doi:10.1016/j.jhydrol.2010.06.042.

Ragettli, S., F. Pellicciotti, R. Bordoy, and W. W. Immerzeel, 2013: Sources of uncertainty in modeling the glaciohydrological

response of a Karakoram watershed to climate change. *Water Resour. Res.*, **49**, 6048–6066, doi:10.1002/wrcr.20450.

Ryu, J. H., J. H. Lee, S. Jeong, S. K. Park, and K. Han, 2011: The impacts of climate change on local hydrology and low flow frequency in the Geum River basin, Korea. *Hydrol. Processes*, **25**, 3437–3447, doi:10.1002/hyp.8072.

Savitskiy, A. G., M. Schlüter, R. V. Taryannikova, N. A. Agaltseva, and V. E. Chub, 2008: Current and future impacts of climate change on river runoff in the central Asian river basins. *Adaptive and Integrated Water Management*, C. Pahl-Wostl, P. Kabat, and G. J. Mölgen, Eds., Springer, 323–339, doi:10.1007/978-3-540-75941-6_17.

Sen, P. K., 1968: Estimates of the regression coefficient based on Kendall's tau. *J. Amer. Stat. Assoc.*, **63**, 1379–1389, doi:10.1080/01621459.1968.10480934.

Sheffield, J., G. Goteti, and E. F. Wood, 2006: Development of a 50-year high-resolution global dataset of meteorological forcings for land surface modeling. *J. Climate*, **19**, 3088–3111, doi:10.1175/JCLI3790.1.

Siegfried, T., T. Bernauer, R. Guiennet, S. Sellars, A. W. Robertson, J. Mankin, P. Bauer-Gottwein, and A. Yakovlev, 2012: Will climate change exacerbate water stress in central Asia? *Climatic Change*, **112**, 881–899, doi:10.1007/s10584-011-0253-z.

Sorg, A., T. Bolch, M. Stoffel, O. Solomina, and M. Beniston, 2012: Climate change impacts on glaciers and runoff in Tien Shan (central Asia). *Nat. Climate Change*, **2**, 725–731, doi:10.1038/nclimate1592.

——, M. Huss, M. Rohrer, and M. Stoffel, 2014: The days of plenty might soon be over in glacierized central Asian catchments. *Environ. Res. Lett.*, **9**, doi:10.1088/1748-9326/9/10/104018.

Stulina, G., and O. Eshchanov, 2013: Climate change impacts on hydrology and environment in the Pre-Aral region. *Quat. Int.*, **311**, 87–96, doi:10.1016/j.quaint.2013.07.015.

Unger-Shayesteh, K., S. Vorogushyn, D. Farinotti, A. Gafurov, D. Duethmann, A. Mandychev, and B. Merz, 2013: What do we know about past changes in the water cycle of central Asian headwaters? A review. *Global Planet. Change*, **110**, 4–25, doi:10.1016/j.gloplacha.2013.02.004.

Wang, X., Y. Luo, L. Sun, and Y. Zhang, 2015: Assessing the effects of precipitation and temperature changes on hydrological processes in a glacier-dominated catchment. *Hydrol. Processes*, **29**, 4830–4845, doi:10.1002/hyp.10538.

Yatagai, A., K. Kamiguchi, O. Arakawa, A. Hamada, N. Yasutomi, and A. Kitoh, 2012: APHRODITE: Constructing a long-term daily gridded precipitation dataset for Asia based on a dense network of rain gauges. *Bull. Amer. Meteor. Soc.*, **93**, 1401–1415, doi:10.1175/BAMS-D-11-00122.1.

Zonn, I. S., 2012: Karakum Canal: Artificial river in a desert. *The Turkmen Lake Altyn Asyr and Water Resources in Turkmenistan*, I. S. Zonn and A. G. Kostianoy, Eds., Handbook of Environmental Chemistry, Vol. 28, Springer, 95–106 pp.